Available online at www.sciencedirect.com

ScienceDirect

Current Opinion in Electrochemistry

Review Article

Electrochemistry of nanobubbles

Ruchirange Ranaweera and Long Luo

Abstract

Gas bubble formation is a common phenomenon in numerous electrochemical processes, such as water splitting, chloralkaline process, and fuel cells. Many efforts have been made to understand the behaviors of microsized or larger gas bubbles in electrochemical systems in the past few decades. It was not until recent years that the electrochemistry of nanosized gas bubbles (nanobubbles) has begun receiving attention. In this short review, we summarize recent advances in the field of electrochemistry of nanobubbles, ranging from new fundamental understandings of nanobubble behaviors to the development of novel bubble-based applications inspired by the basic research of nanobubble electrochemistry.

Addresses

Department of Chemistry, Wayne State University, Detroit, MI, 48202, United States

Corresponding author: Luo, Long (long.luo@wayne.edu)

Current Opinion in Electrochemistry 2020, **22:**102–109

This review comes from a themed issue on **Physical and Nano Electrochemistry**

Edited by **Zhong-Qun Tian**

For a complete overview see the Issue and the Editorial

Available online 28 May 2020

https://doi.org/10.1016/j.coelec.2020.04.019

Keywords

Nanoelectrochemsitry, Nanobubble, Bubble nucleation, Electrochemical sensing, Electrocatalysis.

Early studies of electrogenerated nanobubbles using atomic force microscopy

Atomic force microscopy (AFM) is the tool widely used in the early studies of interfacial nanobubbles. Back in 2007, Zhang et al. [1] imaged, for the first time, the formation and growth of H_2 nanobubbles on a bare, highly oriented pyrolytic graphite surface using in situ tapping mode AFM. A follow-up study by Yang et al. [2] shows electrogeneration of O_2 nanobubbles on highly oriented pyrolytic graphite is also possible, albeit at a lower yield than its H_2 counterpart. They found that after the initial growth, the interfacial nanobubbles were in a dynamic equilibrium state, where the nanobubbles do not further grow despite a continuous gas production by electrochemical reactions. More recently, Dollekamp et al. [3] successfully imaged the electrogenerated H_2 nanobubbles between the sheets of graphene and mica. AFM imaging provides direct evidence for the existence of electrogenerated nanobubbles, but it has a couple of limitations. First, there have been concerns about the AFM–bubble interactions affecting the morphology of the surface bubble during the imaging. Second, owing to the limited time resolution of AFM, it is not feasible to use AFM to study the very early stage of the nanobubble formation or the bubble nucleation.

Studies of a single nanobubble using nanoelectrodes and nanopores

Nanoelectrodes are another popular tool for studying the electrochemistry of nanobubbles. Compared with AFM, nanoelectrodes not only offer an unprecedented time resolution but also generate accurate electrochemical signals associated with the formation and stabilization of a single nanobubble, enabling quantitative studies of a single isolated nanobubble. In 2013, Luo and White [4] demonstrated the first experiment of generating a single H_2 nanobubble by reducing H^+ to H_2 at a Pt nanodisk electrode (Figure 1a). The formation of a single nanobubble was detected from the current drop in the cyclic voltammogram caused by the nanobubble blocking the electrode surface (Figure 1b). There are two important discoveries in this study. First, bubble nucleation requires a ~300-fold supersaturation of dissolved H_2 near the electrode surface, as derived from the peak current value of the voltammogram (i_{nb}^{p}). Second, an electrogenerated nanobubble is likely to be stabilized on the electrode surface by a dynamic steady state, where the loss of H_2 owing to the diffusion from the bubble to the bulk solution is balanced by the electrogenerated H_2 (Figure 1a), as supported by the presence of a residual current after bubble formation (i_{nb}^{r}). The follow-up studies using nanoelectrodes are mainly focused on gaining an in-depth and comprehensive understanding of these two initial discoveries.

Luo et al. [4] continued investigating the effects of electrode sizes and shape on bubble nucleation. They found that the supersaturation level of dissolved H_2 required by bubble nucleation was independent of the nanoelectrode size [5] and shape [6]. Similar studies

This review summarizes recent advances in the field of electrochemistry of nanobubbles.

Figure 1

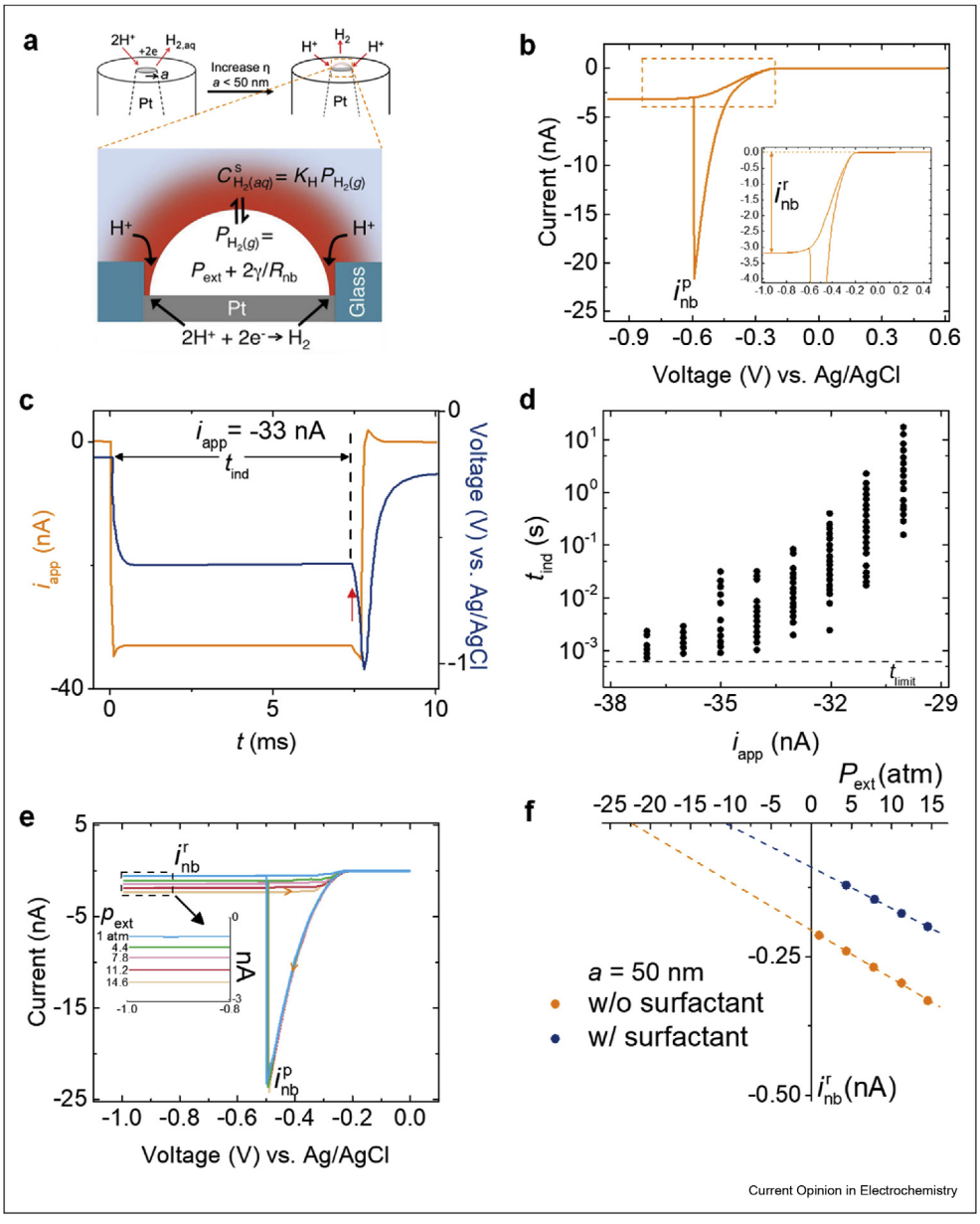

a) Illustration of electrogeneration of a single nanobubble at a Pt nanodisk electrode and the dynamic steady state of an electrogenerated nanobubble. (**b**) A typical cyclic voltammogram recorded for a Pt nanodisk electrode. The peak current at which nanobubble formation occurs is labeled as i^p_{nb}. The inset shows a residual current, i^r_{nb}, after the formation of a nanobubble. (**c**) A current-controlled experiment for studying the dynamics of bubble nucleation. The current is stepped from 0 nA to i_{app} = –33 nA (orange), whereas the potential is monitored (blue). The rapid increase in the potential at ~7.5 ms (indicated by a red arrow) corresponds to the nucleation of a single H_2 nanobubble. (**d**) A plot of the induction time for bubble nucleation, t_{ind}, vs. the set current i_{app}. (**e**) A series of cyclic voltammograms for a Pt nanoelectrode as a function of applied external pressure, P_{ext}. Insert: the expansion of the residual current region of the cyclic voltammograms. (**f**) A plot of i^r_{nb}, vs. P_{ext} with and without surfactant. The absolute value of the *x*-intercept of the regression line gives the Laplace pressure of a nanobubble. Adapted with permission from a study by Luo and White [4] and German et al. [15 and 25], copyright (2013, 2018, and 2016) by the American Chemical Society.

have also been carried out for other gases, including O_2 [5,7,8], N_2 [9], and CO_2 [10], which were electrochemically generated by oxidation of H_2O_2, N_2H_4, and $HCOO^-$, respectively. The nucleation conditions for various gases have been summarized in a recent review article by German et al. [11] Later, Chen and Luo [12] and Chen et al. [13] discovered that the nucleation condition for H_2 bubbles was very similar using Pt, Au, and Pd nanoelectrodes. This finding is interesting because these three metals have significantly different

affinities to H_2 [14], and one would expect the nucleation condition to differ if bubble nucleation follows a heterogeneous nucleation mechanism. The aforementioned studies are based on cyclic voltammetry of nanoelectrodes. Although it has been noticed that i^{p}_{nb} slightly increases at higher scan rates and the value of i^{p}_{nb} also varies somewhat during multiple potential cycles for the same Pt nanoelectrode [4], it was sophisticated to extract information about bubble nucleation from these variabilities in i^{p}_{nb} because of the transient nature of voltammetry. To overcome this challenge, German et al. [15] devised an innovative controlled current experiment. In this experiment, they held a constant current for proton reduction and monitored the potential change (Figure 1c). As the current was stepped to a set value, the potential showed a rapid increase, indicating the start of proton reduction. After a certain period, the potential showed another rapid increase (red arrow in Figure 1c), which corresponds to the formation of a nanobubble. The induction time for bubble nucleation was estimated from the time between the two potential steps. They found that the induction time decreased by ~3 orders of magnitude with only a ~10% increase in the dissolved-gas supersaturation level, which is consistent with the Arrhenius law describing an exponential relationship between bubble nucleation rate and the activation energy (in this case, the supersaturation level). More interestingly, there is a stochastic spread of individual induction times at each current (Figure 1d). Analysis of the cumulative probability, $P(t)$, for the induction time at each current reveals the bubble nucleation at a nanoelectrode can be described by a Poisson process. The data fitting result shows the nucleation of H_2 bubbles is heterogeneous with a contact angle of ~150° and a radius of curvature of ~5 nm for the critical bubble nuclei on the electrode surface. Using these geometric parameters and Henry's law, the number of gas molecules in a bubble nucleus was estimated to be between 35 and 55. A similar heterogeneous nucleation mechanism has also been found for O_2 nanobubbles [7]. Most recently, Edwards et al. [16] revisited the variability of i^{p}_{nb} in the cyclic voltammograms and developed a theoretical model for directly obtaining the properties of bubble nuclei from the distribution of i^{p}_{nb}, which has led to similar conclusions as the controlled current experiments.

The stability of nanobubbles has been a long-argued topic in the interfacial nanobubble community [17,18]. Theoretical prediction has been that bubbles at nanoscale dissolve very quickly owing to the fast kinetics of gas dissolution into the surrounding aqueous phase, which is driven by the high Laplace pressures of nanobubbles. However, the experimentally observed lifetimes of interfacial nanobubbles on a hydrophobic surface were surprisingly long (for many hours). There are several proposed theories to explain this discrepancy between theoretical prediction and experimental observation, including contamination (impurity theory) [19], dynamic steady-state theory [20,21], contact line pinning theory [18], internal pressure theory [22], and gas density theory [23]. The results from the nanoelectrode experiments are in favor of the dynamic steady-state theory. The presence of a residual current after bubble formation (i^{r}_{nb}) in the cyclic voltammogram suggests the need of a continuous supply of H_2 to maintain a stable nanobubble on a nanoelectrode. After removal of this current (by stepping to a positive potential), the nanobubble dissolves quickly, and the lifetime of a H_2 nanobubble was measured to be from a few ms to tens of ms, depending on the nanoelectrode size, by electrochemical means [24]. It was also found that N_2 nanobubbles had a three times longer lifetime than the H_2 bubble generated form the same electrode size because N_2 has a lower solubility and smaller diffusion coefficient than H_2. These findings confirmed that the dissolution of nanobubbles was caused by the diffusional loss of gas from the nanobubble to the bulk solution and $i^{r}_{nb}$was required to compensate this loss. As i^{r}_{nb} is a descriptor of the dynamic steady state of the nanobubble, German et al. [25] designed a creative pressure-addition electrochemical experiment to extract the nanobubble's Laplace pressure from the i^{r}_{nb} values. This experiment is analogous to a standard addition experiment used in analytical chemistry whereby the standard is added directly to the aliquots of the analyzed sample. Instead, they applied different external pressures to affect the dynamic steady state of a nanobubble and recorded the i^{r}_{nb} values (Figure 1e). The x-intercept of the regression line gives the negative of the Laplace pressure of a nanobubble where the H_2 flux is theoretically zero (Figure 1f). In the presence of surfactants, the nanobubble pressure drops because the reduced surface tension leads to a lowered Laplace pressure.

In parallel to the experimental efforts, Perez Sirkin et al. [26] have also started using molecular simulations to elucidate the mechanisms of nucleation and stationary states of electrogenerated nanobubbles at nanoelectrodes. One important finding is that the formation of a stable nanobubble on a nanoelectrode completes within ~20 ns once the cluster of gas molecules exceeds a critical size of ~0.5 nm, which contains ~30 gas molecules. The critical bubble cluster size is in good agreement with the experimentally estimated number of gas molecules in a bubble nucleus [15,16].

Similar to nanoelectrodes, nanopores were also used to detect single nanobubbles taking advantage of their nanosized geometry. The Long group [27–31] has pioneered this method. Figure 2a shows a typical experimental setup, where a nanopore separates a $NaBH_4$ solution and a buffer solution. The two solutions mix at the nanopore orifice and react to generate H_2 nanobubbles. The gas bubble blocks the nanopore orifice, enabling the label-free electrochemical

Figure 2

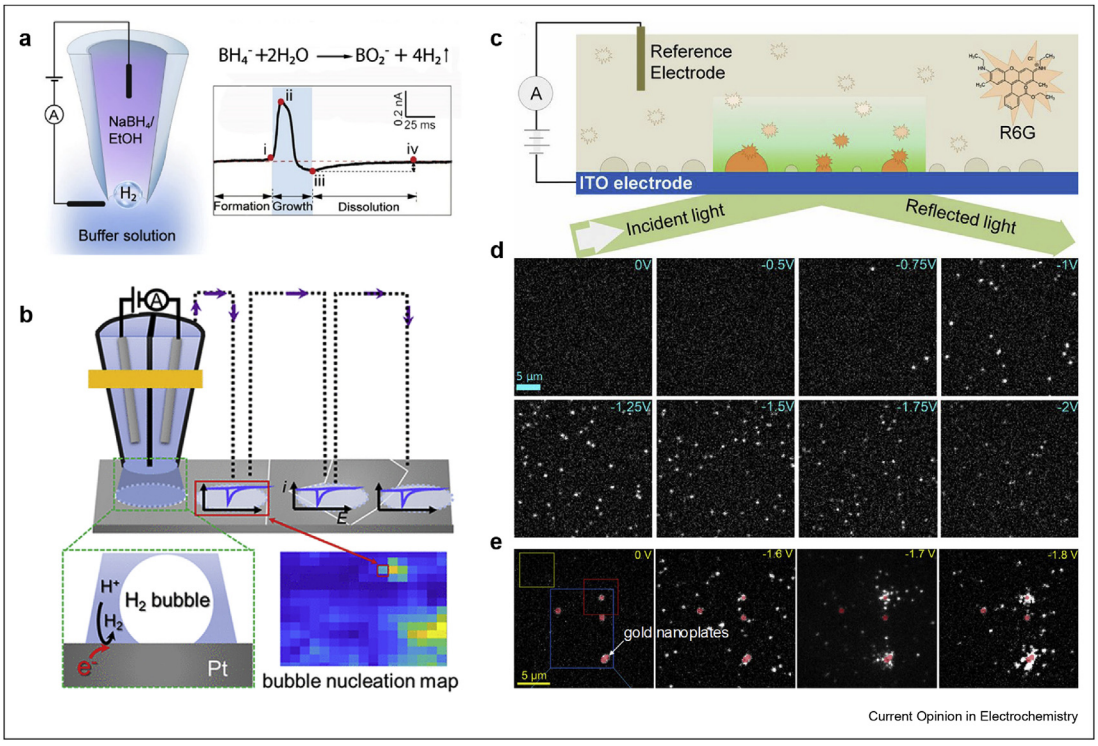

a) Schematic of the experimental setup for analyzing the dynamics of chemically generated nanobubbles using a nanopore, and a typical current–time trace showing the formation (i), growth (i–iii), and dissolution (iii–iv) of a nanobubble. (**b)** The SECCM setup for mapping the H_2 bubble nucleation conditions on an electrocatalytic surface. A nanopipette/droplet probe is drawn near and retracted at different locations to obtain local voltammograms of bubble nucleation. (**c)** Schematic of the experimental setup utilized for imaging surface H_2 nanobubbles during electrocatalytic water splitting. H_2 nanobubbles generated on an indium tin oxide (ITO) surface are labeled by single rhodamine 6G molecules and imaged by total internal reflection fluorescence microscopy. (**d)** A series of fluorescence images of an ITO electrode taken during a potential scan from 0 V to –2.0 V vs. Pt quasi-reference electrode. (**e**) Fluorescence images showing H_2 nanobubbles on a gold nanoplate–decorated ITO electrode in the water at a potential from +0.5 V to –1.8 V vs. Pt quasi-reference electrode. Adapted with permission from a study by Hu et al. [27] and Wang et al. [32] copyright (2018 and 2019) by the American Chemical Society, and from a study by Hao et al. [43], copyright (2018) by the National Academy of Sciences.

detection of chemically generated nanobubbles. A similar idea was adapted by Wang et al. [32] and Perera et al. [33] in their studies of hydrogen evolution reaction activity on a catalytic surface using scanning electrochemical cell microscopy (SECCM). In SECCM, a nanopipette containing electrolyte was used as a probe and scanned across an electrocatalytic surface to evaluate H_2 bubble nucleation conditions. Then, the nucleation condition was correlated with the local hydrogen evolution catalytic activity (Figure 2b). Wang et al. [32] found the dissolved H_2 concentration required for nucleating an H_2 bubble was heterogeneous on a polycrystalline Pt surface, and the variation in activation energy for nucleation was not correlated with the grains or grain boundaries of Pt.

Recent optical microscopic studies of nanobubbles

Both nanoelectrodes and nanopores are great tools for studying single nanobubbles. However, they cannot capture the motions of multiple nanobubbles simultaneously for studying the interbubble interactions, which are common on a real-world electrocatalytic surface. For this job, optical microscopy is the right tool. Various optical microscopic techniques, including optical interference–enhanced reflection microscopy [34], surface plasmon resonance microscopy [35,36], dark-field microscopy [37,38], and total internal reflection fluorescence microscopy [39–42], have been previously used to image interfacial nanobubbles generated by chemical or thermal methods (e.g., laser heating, solvent exchange, catalytic formate decomposition, and photocatalytic water reduction).

Recently, these microscopic techniques were adapted and modified for investigating the electrochemistry of nanobubbles. For example, Hao et al. [43] used total internal reflection fluorescence microscopy to study H_2 nanobubbles at the electrode/solution interface produced by water reduction (Figure 2c). Imaging of these surface nanobubbles was enabled by fluorescence dye

molecules (e.g., Rhodamine 6G) that can be momentarily trapped at the nanobubble's gas/solution interface. They found that each nanobubble mostly had one single fluorescent molecule label, and the number of H_2 nanobubbles increased as the electrode potential became more negative (Figure 2d). When the indium tin oxide (ITO) electrode was decorated by catalytic gold nanoplates, they observed that H_2 nanobubbles appeared not only around the more catalytic gold nanoplates but also on the less catalytic ITO surface at

Figure 3

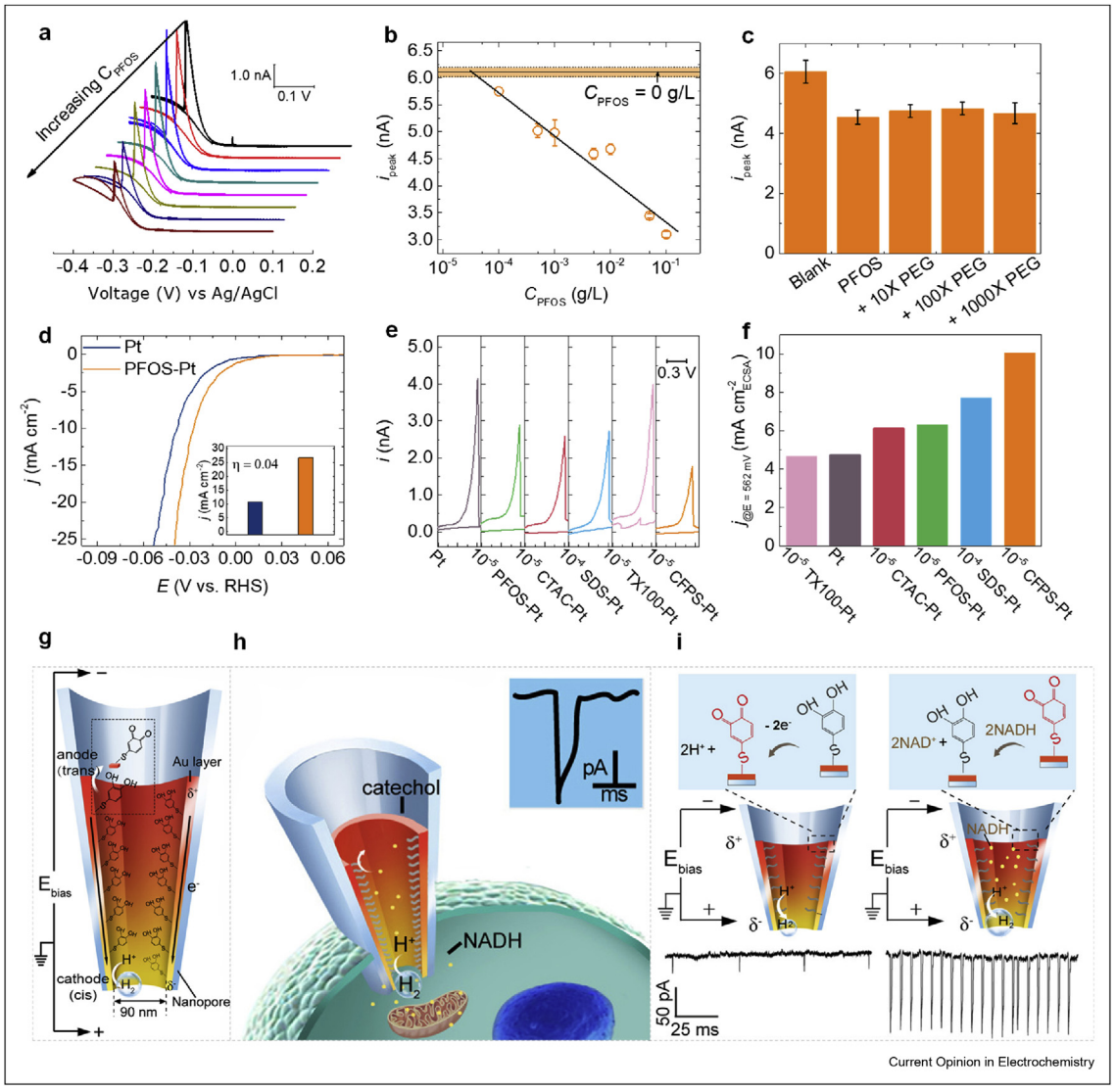

a) Cyclic voltammograms of a Pt nanoelectrode at different perfluorooctanesulfonate (PFOS) concentrations from 0 to 10^{-1} g/L. (**b**) The peak currents in (**a**), i_{peak}, as a function of C_{PFOS}. (**c**) Comparison of i_{peak} in the presence of 1.0 mg/L PFOS, and after the addition of a 10- to 1000-fold excess of poly(ethylene glycol) (PEG, 400 g/mol). (**d**) Polarization curves of PFOS-Pt and pure Pt in N_2-saturated 0.5 M $HClO_4$ solution. The inset shows the current densities of PFOS-Pt and pure Pt at an overpotential of 0.04 V. (**e**) Cyclic voltammograms of a Pt nanoelectrode in a hydrazine solution containing different surfactants (including PFOS, cationic fluorinated pyridinium sulfonate (CFPS), cetrimonium chloride (CTAC), sodium dodecyl sulfate (SDS), and TritonX-100 (TX100)). (**f**) Comparison of hydrazine oxidation current densities for different surfactant-modulated Pt at a fixed potential of 562 mV vs. RHE. (**g**) Illustration of an asymmetric nanopore electrode (ANE) for probing redox-active species. The applied bias potential (E_{bias}) provides the potential difference at the two ends of the Au coating on the interior wall of the nanopore, driving the oxidation of catechol to *o*-benzoquinone and the proton reduction to H_2. (**h**) The ANE for single-cell probing. The intracellular redox specie (e.g., NADH) diffuses into the ANE and reacts. (**i**) The catechol-modified ANE generates a current signal due to the formation of H_2 nanobubbles blocking the nanopore orifice. In the presence of NADH, the catechol/o-benzoquinone conversion is turned over by NADH, leading to an increased current response with a high amplitude. Adapted with permission from a study by Ying et al. [31] and Ranaweera et al. [45], copyright (2018 and 2019) by the American Chemical Society, from a study by Zhao et al. [49], copyright (2019) by the Royal Society of Chemistry, and from ref 50, copyright (2019) by Wiley-VCH.

small overpotentials; at high overpotentials, the nanobubbles started gathering around the gold nanoplates (Figure 2e). This behavior was attributed to the hydrogen spillover in which H atoms generated on a catalyst surface migrate out onto the support substrate, leading to significant bubble formation on the ITO surface. Most recently, Hao et al. [44] extended this approach to the study of H_2 and O_2 nanobubbles on Au/Pd alloy—modified ITO electrode.

Applications inspired by the fundamental studies of nanobubble electrochemistry

The goal of fundamental research is to generate new knowledge for future applications. Already, the findings from the fundamental studies of nanobubble electrochemistry have inspired several bubble-based applications. For example, the Ranaweera et al. [45] have developed a bubble nucleation—based electrochemical method for the selective and sensitive detection of surfactants. This method is based on the nanoelectrode platform previously discussed in Figure 1. It relies on the high surface activity of surfactant analytes to affect the electrochemical bubble nucleation. When surfactant concentration increases, the solution surface tension decreases lowering the nucleation energy barrier and reducing bubble nucleation current (Figure 3a). Using this method, they demonstrated the quantitation of perfluorinated surfactants in water, a group of emerging environmental contaminants, with a remarkable limit of detection down to 30 μg/L and a linear dynamic range of more than 3 orders of magnitude (Figure 3b). The experimental results are in quantitative agreement with the theoretical model they derived from classical nucleation theory. This bubble nucleation—based method exhibits an exceptional specificity for the surfactant analytes, even in the presence of 1000-fold excess of nonsurfactant interference, such as poly(-ethylene glycol) (Figure 3c).

Another bubble-based application is related to electrochemical gas evolution reactions. During gas evolution reactions, the electrolyte solution near electrodes is supersaturated with dissolved gas. The interfacial supersaturation level can reach as high as 300 to 400 [46]. According to the Nernst equation, such a high local concentration of the product (in this case, dissolved gas) on the electrode surface causes a concentration overpotential [47,48]. Zhao et al. [49] discovered that fluorinated surfactants were effective in promoting H_2 bubble nucleation and lowering the interfacial dissolved gas concentration while minimizes the blockage of surface catalytic sites. As a result, the addition of perfluorooctanesulfonate (PFOS—Pt) caused a significant positive shift of the polarization curve for hydrogen evolution, compared with the pure Pt catalyst (Figure 3d). This finding is exciting because Pt is known to be the best electrocatalyst for hydrogen evolution reaction in acids; now, the use of PFOS breaks the 'glass ceiling' of catalytic performance. After achieving this remarkable performance for the hydrogen evolution reaction, Zhao et al. [50] further applied this strategy to the hydrazine oxidation reaction. They found that there was a direct positive correlation between the ability to promote bubble nucleation and the ability to improve the hydrazine oxidation performance for surfactants (Figure 3e and f). Among 5 different surfactants (PFOS, cationic fluorinated pyridinium sulfonate, cetrimonium chloride, sodium dodecyl sulfate, and TritonX-100), cationic fluorinated pyridinium sulfonate is most effective in reducing the N_2 bubble nucleation current and in promoting hydrazine oxidation (Figure 3e and f).

Nanopore-based nanobubble studies have also led to new applications. For example, Ying et al. [31] designed an asymmetric nanopore electrode (ANE) that uses nanobubble formation to amplify the signal for monitoring electron transfer dynamics in live cells. In this ANE design, a thin gold coating on the interior wall of the ANE is modified by redox-active molecules, that is, catechol (Figure 3g). When a positive voltage bias is applied between outside and inside the nanopore, the gold coating acts as a bipolar electrode, driving the oxidation of catechol to *o*-benzoquinone and the proton reduction to H_2 at the two ends of the gold coating (Figure 3h). In the presence of NADH, an intracellular redox species, the catechol/*o*-benzoquinone conversion can be turned over, leading to significantly increased H_2 generation and nanobubble formation, which amplifies the electrochemical signal by blocking the nanopore orifice (Figure 3i). The ANE achieves the highly sensitive and selective probing of NADH concentrations as low as 1 pM, enabling the real-time monitoring of the respiration chain (i.e., NADH) in a living cell and the evaluation of the effects of anticancer drugs in an MCF-7 cell.

Conclusions and future directions for the field

In conclusion, this short review summarizes advances in the field of electrochemistry of nanobubbles, ranging from new fundamental understandings of their behaviors to some novel bubble-based applications stemming from the basic research of nanobubble electrochemistry. Despite these advances, there are still many unanswered questions in this field, especially about the roles of nanobubbles in electrocatalytic systems. For example, the work by Hao et al. [43] has clearly shown the H_2 nanobubbles are constantly present on the catalytic surface during hydrogen evolution reaction — and the nanobubbles also behave differently from what one would expect. However, it is unclear how these nanobubbles affect catalytic performance. In addition, prior electrocatalysis studies have shown the presence of macroscopic gas bubbles on a catalytic surface can

drastically change the product selectivity of an electrocatalytic reaction [51,52]. Then, how about electrogenerated nanobubbles? Will they have the same effects? The work by Zhao et al. [49,50] has shown an interesting empirical correlation between bubble nucleation and catalytic activity for a gas evolution reaction, but what is exactly happening on the catalytic surface? In our opinion, the main challenges in studying the roles of nanobubbles in real electrocatalytic systems are three-fold. First, it is difficult to image surface nanobubbles on an electrocatalytic surface with high time and spatial resolutions. Second, it is even more challenging to identify the electrocatalytic reaction products around a surface nanobubble, which provides direct evidence for investigating the nanobubble-induced product selectivity change. Third, even when these tools for studying the nanobubbles are well established, it will not be trivial to correlate the results from nanoscopic and macroscopic measurements. There is no doubt that it is much challenging to study these complicated catalytic systems, but it is also rewarding.

Declaration of Competing Interest

The authors declare that they have no competing financial interests or personal relationships that could have appeared to influence the work reported in this article.

Acknowledgements

RR and LL gratefully acknowledge support from Chemical Measurement & Imaging Program, National Science Foundation (Award # CHE-1943737), and the start-up funds from Wayne State University.

References

Papers of particular interest, published within the period of review, have been highlighted as:

* * of outstanding interest

1. Zhang L, Zhang Y, Zhang X, Li Z, Shen G, Ye M, Fan C, Fang H, Hu J: **Electrochemically controlled formation and growth of hydrogen nanobubbles**. *Langmuir* 2006, **22**:8109–8113.
2. Yang S, Tsai P, Kooij ES, Prosperetti A, Zandvliet HJ, Lohse D: **Electrolytically generated nanobubbles on highly orientated pyrolytic graphite surfaces**. *Langmuir* 2009, **25**:1466–1474.
3. Dollekamp E, Bampoulis P, Poelsema B, Zandvliet HJW, Kooij ES: **Electrochemically induced nanobubbles between graphene and mica**. *Langmuir* 2016, **32**:6582–6590.
4. Luo L, White HS: **Electrogeneration of single nanobubbles at sub-50-nm-radius platinum nanodisk electrodes**. *Langmuir* 2013, **29**:11169–11175.
5. Chen Q, Luo L, Faraji H, Feldberg SW, White HS: **Electrochemical measurements of single H_2 nanobubble nucleation and stability at Pt nanoelectrodes**. *J Phys Chem Lett* 2014, **5**:3539–3544.
6. Chen QJ, Luo L, White HS: **Electrochemical generation of a hydrogen bubble at a recessed platinum nanopore electrode**. *Langmuir* 2015, **31**:4573–4581.
7. Soto AM, German SR, Ren H, van der Meer D, Lohse D, Edwards MA, White HS: **The nucleation rate of single O_2 nanobubbles at Pt nanoelectrodes**. *Langmuir* 2018, **34**:7309–7318.
8. Ren H, German SR, Edwards MA, Chen Q, White HS: **Electrochemical generation of individual O_2 nanobubbles via H_2O_2 oxidation**. *J Phys Chem Lett* 2017, **8**:2450–2454.
9. Chen Q, Wiedenroth HS, German SR, White HS: **Electrochemical nucleation of stable N_2 nanobubbles at Pt nanoelectrodes**. *J Am Chem Soc* 2015, **137**:12064–12069.
10. Ren H, Edwards MA, Wang Y, White HS: **Electrochemically controlled nucleation of single CO_2 nanobubbles via formate oxidation at Pt nanoelectrodes**. *J Phys Chem Lett* 2020, **11**:1291–1296.
11. German SR, Edwards MA, Chen Q, Liu Y, Luo L, White HS: **Electrochemistry of single nanobubbles. Estimating the critical size of bubble-forming nuclei for gas-evolving electrode reactions**. *Faraday Discuss* 2016, **193**:223–240.
12. Chen QJ, Luo L: **Correlation between gas bubble formation and hydrogen evolution reaction kinetics at nanoelectrodes**. *Langmuir* 2018, **34**:4554–4559.
13. Chen Q, Ranaweera R, Luo L: **Hydrogen bubble formation at hydrogen–insertion electrodes**. *J Phys Chem C* 2018, **122**:15421–15426.
14. Greeley J, Jaramillo TF, Bonde J, Chorkendorff IB, Norskov JK: **Computational high-throughput screening of electrocatalytic materials for hydrogen evolution**. *Nat Mater* 2006, **5**:909–913.
15. * * German SR, Edwards MA, Ren H, White HS: **Critical nuclei size, rate, and activation energy of H_2 gas nucleation**. *J Am Chem Soc* 2018, **140**:4047–4053.

This work describes the theory of electrochemical nucleation of gas bubbles and the use of this theory and experimental data to obtain the properties of bubble nuclei.

16. Edwards MA, White HS, Ren H: **Voltammetric determination of the stochastic formation rate and geometry of individual H_2, N_2, and O_2 bubble nuclei**. *ACS Nano* 2019, **13**:6330–6340.
17. Sun Y, Xie G, Peng Y, Xia W, Sha J: **Stability theories of nanobubbles at solid–liquid interface: a review**. *Colloids Surf, A* 2016, **495**:176–186.
18. Zhang X, Chan DY, Wang D, Maeda N: **Stability of interfacial nanobubbles**. *Langmuir* 2013, **29**:1017–1023.
19. Ducker WA: **Contact angle and stability of interfacial nanobubbles**. *Langmuir* 2009, **25**:8907–8910.
20. Brenner MP, Lohse D: **Dynamic equilibrium mechanism for surface nanobubble stabilization**. *Phys Rev Lett* 2008, **101**:214505.
21. Seddon JR, Zandvliet HJ, Lohse D: **Knudsen gas provides nanobubble stability**. *Phys Rev Lett* 2011, **107**:116101.
22. Zhang XH, Quinn A, Ducker WA: **Nanobubbles at the interface between water and a hydrophobic solid**. *Langmuir* 2008, **24**:4756–4764.
23. Zhang LJ, Chen H, Li ZX, Fang HP, Hu J: **Long lifetime of nanobubbles due to high inner density**. *Sci China, Ser A G* 2008, **51**:219–224.
24. German SR, Chen QJ, Edwards MA, White HS: **Electrochemical measurement of hydrogen and nitrogen nanobubble lifetimes at pt nanoelectrodes**. *J Electrochem Soc* 2016, **163**:H3160–H3166.
25. German SR, Edwards MA, Chen Q, White HS: **Laplace pressure of individual H_2 nanobubbles from pressure-addition electrochemistry**. *Nano Lett* 2016, **16**:6691–6694.
26. * * Perez Sirkin YA, Gadea ED, Scherlis DA, Molinero V: **Mechanisms of nucleation and stationary states of electrochemically generated nanobubbles**. *J Am Chem Soc* 2019, **141**:10801–10811.

This work is the first molecular dynamics study of electrogenated nanobubbles.

27. Hu YX, Ying YL, Gao R, Yu RJ, Long YT: **Characterization of the dynamic growth of the nanobubble within the confined glass nanopore**. *Anal Chem* 2018, **90**:12352–12355.
28. Li Q, Ying YL, Hu YX, Liu SC, Long YT: **Monitoring nanobubble nucleation at early-stage within a sub-9 nm solid-state**

nanopore. *Electrophoresis* 2019, https://doi.org/10.1002/elps.201900305.

29. Li Q, Ying YL, Liu SC, Hu YX, Long YT: **Measuring temperature effects on nanobubble nucleation via a solid-state nanopore**. *Analyst* 2020, https://doi.org/10.1039/d0an00041h.

30. Gao R, Ying YL, Hu YX, Li YJ, Long YT: **Wireless bipolar nanopore electrode for single small molecule detection**. *Anal Chem* 2017, **89**:7382–7387.

31. ** Ying YL, Hu YX, Gao R, Yu RJ, Gu Z, Lee LP, Long YT: **Asymmetric nanopore electrode-based amplification for electron transfer imaging in live cells**. *J Am Chem Soc* 2018, **140**:5385–5392.
This work demonstrates a novel use of nanobubble formation in nanopores as a signal amplification method.

32. Wang Y, Gordon E, Ren H: **Mapping the nucleation of H_2 bubbles on polycrystalline Pt via scanning electrochemical cell microscopy**. *J Phys Chem Lett* 2019, **10**:3887–3892.

33. Perera RT, Arcadia CE, Rosenstein JK: **Probing the nucleation, growth, and evolution of hydrogen nanobubbles at single catalytic sites**. *Electrochim Acta* 2018, **283**:1773–1778.

34. Karpitschka S, Dietrich E, Seddon JR, Zandvliet HJ, Lohse D, Riegler H: **Nonintrusive optical visualization of surface nanobubbles**. *Phys Rev Lett* 2012, **109**, 066102.

35. Chen J, Zhou K, Wang Y, Gao J, Yuan T, Pang J, Tang S, Chen HY, Wang W: **Measuring the activation energy barrier for the nucleation of single nanosized vapor bubbles**. *Proc Natl Acad Sci Unit States Am* 2019, **116**:12678–12683.

36. Wang Y, Chen J, Jiang Y, Wang X, Wang W: **Label-free optical imaging of the dynamic stick-slip and migration of single sub-100-nm surface nanobubbles: a superlocalization approach**. *Anal Chem* 2019, **91**:4665–4671.

37. Zhang T, Li S, Du Y, He T, Shen Y, Bai C, Huang Y, Zhou X: **Revealing the activity distribution of a single nanocatalyst by locating single nanobubbles with super-resolution microscopy**. *J Phys Chem Lett* 2018, **9**:5630–5635.

38. Li S, Du Y, He T, Shen Y, Bai C, Ning F, Hu X, Wang W, Xi S, Zhou X: **Nanobubbles: an effective way to study gas-generating catalysis on a single nanoparticle**. *J Am Chem Soc* 2017, **139**:14277–14284.

39. Chan CU, Ohl CD: **Total-internal-reflection-fluorescence microscopy for the study of nanobubble dynamics**. *Phys Rev Lett* 2012, **109**:174501.

40. Chan CU, Arora M, Ohl CD: **Coalescence, growth, and stability of surface-attached nanobubbles**. *Langmuir* 2015, **31**:7041–7046.

41. Tan BH, An H, Ohl CD: **Resolving the pinning force of nanobubbles with optical microscopy**. *Phys Rev Lett* 2017, **118**, 054501.

42. Su H, Fang Y, Chen F, Wang W: **Monitoring the dynamic photocatalytic activity of single CdS nanoparticles by lighting up H_2 nanobubbles with fluorescent dyes**. *Chem Sci* 2018, **9**:1448–1453.

43. ** Hao R, Fan Y, Howard MD, Vaughan JC, Zhang B: **Imaging nanobubble nucleation and hydrogen spillover during electrocatalytic water splitting**. *Proc Natl Acad Sci Unit States Am* 2018, **115**:5878–5883.
This work describes the experimental setup and method for imaging nanobubbles during electrochemical gas evolution reactions using fluorescence microscopy.

44. Hao R, Fan Y, Anderson TJ, Zhang B: **Imaging single nanobubbles of H_2 and O_2 during the overall water electrolysis with single-molecule fluorescence microscopy**. *Anal Chem* 2020, **92**:3682–3688.

45. ** Ranaweera R, Ghafari C, Luo L: **Bubble-nucleation-based method for the selective and sensitive electrochemical detection of surfactants**. *Anal Chem* 2019, **91**:7744–7748.
This work shows a novel application of electrochemical bubble nucleation in sensitive and selective detection of surfactants.

46. ** Zhao X, Ren H, Luo L: **Gas bubbles in electrochemical gas evolution reactions**. *Langmuir* 2019, **35**:5392–5408.
This work is a comprehensive review of the previous work on gas bubbles in electrochemical systems.

47. Dukovic J, Tobias CW: **The influence of attached bubbles on potential drop and current distribution at gas-evolving electrodes**. *J Electrochem Soc* 1987, **134**:331–343.

48. Vogt H: **The concentration overpotential of gas evolving electrodes as a multiple problem of mass-transfer**. *J Electrochem Soc* 1990, **137**:1179–1184.

49. Zhao X, Ranaweera R, Luo L: **Highly efficient hydrogen evolution of platinum via tuning the interfacial dissolved-gas concentration**. *Chem Commun* 2019, **55**:1378–1381.

50. Zhao X, Ranaweera R, Mixdorf JC, Nguyen HM, Luo L: **Lowering interfacial dissolved gas concentration for highly efficient hydrazine oxidation at platinum by fluorosurfactant modulation**. *ChemElectroChem* 2019, **7**:55–58.

51. Xia C, Back S, Ringe S, Jiang K, Chen FH, Sun XM, Siahrostami S, Chan KR, Wang HT: **Confined local oxygen gas promotes electrochemical water oxidation to hydrogen peroxide**. *Nat Catal* 2020, **3**:125–134.

52. Zhang C, Xu Y, Lu P, Zhang X, Xu F, Shi J: **Capillary effect-enabled water electrolysis for enhanced electrochemical ozone production by using bulk porous electrode**. *J Am Chem Soc* 2017, **139**:16620–16629.